Available online at www.sciencedirect.com

ScienceDirect

Journal of the European Ceramic Society 35 (2015) 1841–1846

www.elsevier.com/locate/jeurceramsoc

Creep behavior of perovskite-type oxides $Ba_{0.5}Sr_{0.5}(Co_{0.8}Fe_{0.2})_{1-x}Zr_xO_{3-\delta}$

V. Stournari [a], S.F.P. ten Donkelaar [b], J. Malzbender [a,*], T. Beck [c], L. Singheiser [a], H.J.M. Bouwmeester [b]

[a] *Forschungszentrum Jülich GmbH, Institute for Energy and Climate Research, IEK-2, 52425 Jülich, Germany*
[b] *University of Twente, Faculty of Science and Technology, Inorganic Membranes, MESA+ Institute for Nanotechnology, Enschede, The Netherlands*
[c] *Technische Universität Kaiserslautern, Lehrstuhl für Werkstoffkunde (WKK), 67663 Kaiserlautern, Germany*

Received 17 October 2014; received in revised form 6 January 2015; accepted 7 January 2015
Available online 22 January 2015

Abstract

Compressive creep tests have been performed on perovskite-type oxides $Ba_{0.5}Sr_{0.5}(Co_{0.8}Fe_{0.2})_{1-x}Zr_xO_{3-\delta}$ (BSCF-Z100·x), where $x = 0.01$, 0.03, 0.05 and 0.1, for the use as oxygen transport membrane, in air at 800–950 °C and at nominal stresses of 30 MPa and 63 MPa. X-ray diffraction and microstructural observations support a solid solubility limit of ZrO_2 between $0.03 < x < 0.05$. Evidence is found for the formation of (Ba,Sr)ZrO_3 secondary phases in grain boundaries at compositions beyond this limit. Zr substitution of (Co,Fe) in BSCF is found to suppress grain growth significantly, which is attributed to a solute and/or particle drag (Zener pinning) mechanism. Observed activation energies and stress exponents point to diffusional creep as the predominant mechanism for creep in BSCF-Z100·x ceramics, at $T \geq 850$ °C. This is further supported by the fact that the grain-size-normalized steady-state creep rate varies little for the different BSCF-Z100·x compositions. It was confirmed that Zr substitution does not significantly affect the thermal hysteresis of the creep behavior as observed for pure BSCF.

Keywords: Creep; Perovskite; BSCF; Zr substitution; Oxygen transport membrane

1. Introduction

The perovskite-type oxide $Ba_{0.5}Sr_{0.5}Co_{0.8}Fe_{0.2}O_{3-\delta}$ (BSCF) has been intensively investigated for its potential use as oxygen transport membrane (OTM). Thin film asymmetric (supported) membranes prepared from BSCF have been found to exhibit unprecedentedly high oxygen fluxes.[1,2] However, the material suffers from stability issues related to its decomposition at moderate temperatures (below ~850 °C)[3] and a limited mechanical stability,[4] noting that a long-term reliability of performance is required that is measured in years.[5,6] One of the critical mechanical parameters is creep as it can lead to structural instability and tensile failure already under low stress exposure.[7] In general, creep behavior is affected by extrinsic and intrinsic parameters, such as stress, temperature and grain size. Data on the dependence of creep on these parameters give important information on the underlying creep mechanism, but also influence design criteria for OTM membranes. Data on the creep properties of various membrane candidate materials can be found in Lipinska et al.[8]

The compressive creep behavior of BSCF has been investigated by Yi et al.[9] and Rutkowski et al.[4,10] Both groups of authors have reported creep deformation of BSCF in the temperature range from 800 to 950 °C to be dominated by cation diffusion via the oxide lattice (bulk) and along grain boundaries. A profound increase of the creep rate is observed above ~850 °C, below which temperature a sluggish decomposition of BSCF occurs into cubic and hexagonal polymorphs. Both cited groups of authors conclude that the presence of hexagonal polymorphs significantly enhances the material's creep resistance. The amount of secondary phases in BSCF is found to depend strongly on the thermal history of the material.[4,10,11] Since the cubic phase is the

* Corresponding author. Tel.: +49 2461616964; fax: +49 2461613699.
E-mail address: j.malzbender@fz-juelich.de (J. Malzbender).

http://dx.doi.org/10.1016/j.jeurceramsoc.2015.01.005
0955-2219/

thermodynamically stable phase above 850 °C, thermal cycling gives rise to a pronounced hysteresis in the creep behavior of BSCF.

The phase instability of BSCF below the critical temperature of ~850 °C as well as its detrimental effect on oxygen transport properties have been studied by different researchers.[12,2,13,14] In general, the results confirm that grain boundaries and/or imperfections, such as cobalt oxide precipitates, serve as sites for nucleation and growth of secondary phases. Using transmission electron microscopy (TEM) techniques, Mueller et al.[14] observed a decomposition of BSCF into hexagonal 2H-$Ba_{0.5+x}Sr_{0.5-x}CoO_{3-\delta}$, and a (relative to pure BSCF) Ba- and Co-depleted cubic perovskite-type phase $Ba_{0.5-x}Sr_{0.5+x}Co_{0.6}Fe_{0.4}O_{3-\delta}$. Efimov et al.[15] suggested hexagonal 2H-$Ba_{0.6}Sr_{0.4}CoO_{3-\delta}$ and a lamellar, non-cubic phase $Ba_{1-x}Sr_xCo_{2-y}Fe_yO_{5\delta}$ as main decomposition products. Extended investigations by Müller et al.[16] identified the latter phase as an intergrowth compound, $Ba_{m+1}Co_mO_{3m+3}$ (Co_8O_8), $m \geq 2$ (denoted by BCO), consisting of CdI_2-type CoO_2 and perovskite layers. Regions with a plate-like morphology were identified, consisting of a random arrangement of cubic (with a small departure of the original BSCF composition), hexagonal, and BCO-type phases.

Several groups have demonstrated that the undesired phase decomposition of BSCF below ~850–900 °C can be avoided by partial substitution of (Co,Fe) by redox-stable cations such as Nb, Y, and Zr, albeit at the expense of the magnitude of the oxygen flux.[17–20] The rational behind these substitutions is Goldschmidt's theory as to the relative stability of cubic and hexagonal perovskite structures,[13] and to avoid a significant increase in the oxygen stoichiometry, and hence lowering of the average oxidation state and concomitant change in the radii of the constituent cations upon lowering the temperature (or increasing the ambient oxygen partial pressure). Recently, it was suggested that the introduction of 3 mol% ZrO_2 would be sufficient to prevent decomposition of BSCF.[20] No sign of performance degradation was found in data of electrical conductivity and conductivity relaxation curves recorded at 800 °C and pO_2 of 1 atm over 260 h. A follow-up study conducted by Ravkina et al.[21] however, demonstrated oxygen permeation fluxes to decline with time when these are recorded at 750 °C.

Results in particular on the elevated temperature mechanical properties of Zr doped BSCF are limited. Mechanical characterization of this composition manufactured by extrusion regarding creep and strength revealed that the thermo-mechanical characteristics of BSCF and BSCF-Z3 mostly agree.[11,22]

The aim of the current study is to investigate the influence of partial substitution of (Co,Fe) by Zr on the creep behavior of BSCF. The creep measurements include compositions beyond the solubility limit of the Zr-dopant in BSCF to study the effect of second phase impurities in the grain boundaries.

2. Experimental

$Ba_{0.5}Sr_{0.5}(Co_{0.8}Fe_{0.2})_{1-x}Zr_xO_{3-\delta}$ (BSCF-Z100·x) powders with $x = 0.01$, 0.03, 0.05, and 0.10 were prepared using a spray pyrolysis technique (CerPoTech, Norway). The as-received powders were ball-milled in ethanol and calcined at 900 °C for 6 h in air. The phase composition of the calcined powders was assessed by X-ray powder diffraction (Philips X'Pert PW3020) with Cu K_α radiation at room temperature. No evidence of second phase formation was found. Green cylinders were obtained by uniaxial pressing at 50 MPa followed by isostatic pressing at 400 MPa. These were subsequently sintered at 1120 °C for 30 h in air to a relative density of more than 95%. Additional annealing studies of BSCF-Z100·x were performed at 850 °C for 336 h in air in order to investigate the phase stability at this temperature.

For creep tests, the sintered cylinders were machined to a length of ~12 mm and a diameter of 6 mm, and their end faces were parallelized by grinding in order to minimize surface effects and superimposed bending by misalignments. Compressive creep tests were performed in ambient air, using an Instron 1362 electromechanical testing machine equipped with a high temperature furnace, under a constant uniaxial load, corresponding to nominal stresses of 30 and 63 MPa. The samples were mounted between two alumina push rods. A linear variable differential transformer (LVDT, Sangami) with range ±1 mm and precision 1.25 μm was used for the vertical displacement measurement. The load was controlled with a 10 kN load cell (Interface 1210 ACK), while the temperature was monitored with a K type thermocouple located near the sample surface.

A typical test run was conducted in the temperature range from 800 to 950 °C, which corresponds to $0.65\,T_m \leq T \leq 0.78\,T_m$ (melting temperature $T_m = 1290$ °C for BSCF[23]). Prior to testing, each sample was pre-annealed at 850 °C for 24 h to ensure defect chemical equilibrium, to eliminate associated strains and minimize influences of hexagonal phases to creep behavior.[4,7] Subsequently, the sample was cooled at a rate of 8 K/min to the first (i.e. lowest) measurement temperature. The temperature was incremented step wise, with 50 K intervals, using heating and cooling rates of 8 K/min. At every measurement temperature, the sample was allowed to equilibrate for 1 h before the actual load was applied. Each creep measurement was terminated after 24 h of steady-state deformation or until an integral deformation of 100 μm was reached. For details on the creep testing procedure and instrumentation, see also Refs. 4 and 10. The strain was calculated from the ratio of measured deformation Δh and initial height h_0:

$$\varepsilon = \frac{\Delta h}{h_0} \tag{1}$$

The steady-state creep rate $\dot{\varepsilon}$ was analyzed using the generalized power law relationship[24]:

$$\dot{\varepsilon} = A \cdot \left(\frac{1}{d}\right)^p \cdot \sigma^n \cdot \exp\left(-\frac{Q}{RT}\right) \tag{2}$$

where d is the grain size, p is the inverse grain size exponent, Q is the apparent activation energy, A is a proportionality parameter, while R and T have their usual meanings. Creep parameters p, n, and Q were obtained by fitting the experimental data obtained for each sample to Eq. (1), using multiple linear regression

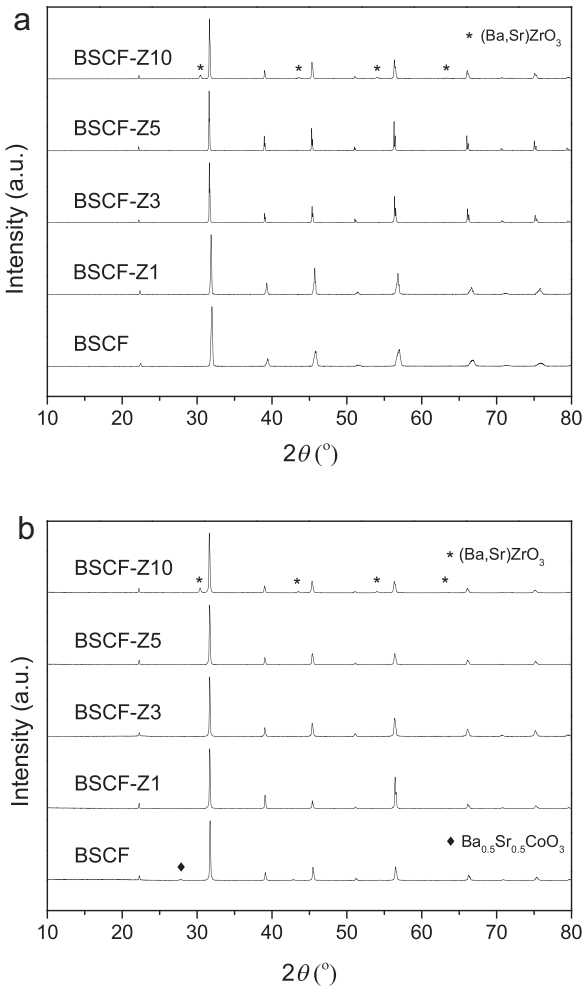

Fig. 1. XRD patterns of sintered compacts of BSCF-Z100·x (a) before and (b) after annealing in air, at 850 °C, for 336 h. Reflections for (Ba,Sr)ZrO_3 and hexagonal $Ba_{0.5}Sr_{0.5}CoO_3$ are indicated.

analysis. Structural investigations of the crystalline phases before and after the creep tests were carried out using an X-ray diffractometer (D4 Endeavor, Bruker AXS, Germany) with Cu-K_α radiation. A continuous scan mode was used to collect data in the 2θ range 10–130° with a 0.01° step size and a 5 s/step counting time. Microstructural characterizations of the samples in an as-received, deformed and/or fractured state were performed using scanning electron microscopy (SEM, Zeiss SUPRA 50VP and Zeiss Merlin). Elemental analysis was carried out by EDX (Inca, Oxford Instruments). Electron backscatter diffraction (EBSD) was performed to determine the grain orientation before and after the creep test for BSCF-Z10. To reveal the grain boundaries, longitudinal sections were cut from the samples and mechanically polished down to 0.25 μm diamond paste. To investigate microstructural changes induced by creep deformation, longitudinal sections parallel to the loading axis were cut from the central part of the samples. The AnalysisPro© software package was used for estimation of the grain size. Since the linear intercept and equivalent circular diameter (ECD) methods revealed good agreement in initial tests, the more simple ECD method was used in subsequent analyses.

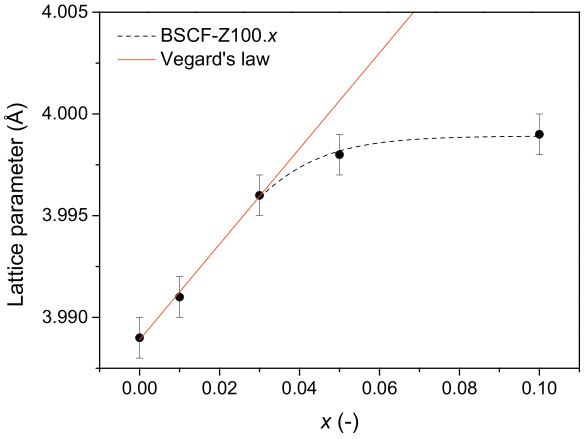

Fig. 2. Evolution of the lattice parameter with x in BSCF-Z100·x. The dashed line indicates Vegard's law for solid solution.

Table 1
Average grain size (equivalent circular diameter – ECD) along with standard deviations (s.d.) for BSCF-Z100·x after sintering.

	Grain size [μm]
BSCF	17.0 (6.0)
BSCF[a]	29.0 (11.0)
BSCF-Z1	17.0 (4.0)
BSCF-Z3	8.0 (2.0)
BSCF-Z5	5.0 (2.0)
BSCF-Z10	1.5 (0.5)

[a] Data from Ref. 4.

3. Results and discussion

3.1. Solid solubility limit and microstructure

Fig. 1 shows XRD patterns collected at room temperature of sintered samples BSCF-Z100·x before and after annealing at 850 °C in air for 336 h. Diffraction patterns of both series can be indexed using a cubic perovskite structure. In the patterns obtained for BSCF-Z10, peaks of a secondary phase can be assigned to (Ba,Sr)ZrO_3 [PDF 00-006-0399]. The peak at 27.8° in the pattern obtained for pure BSCF can be assigned to hexagonal $Ba_{0.5}Sr_{0.5}CoO_3$ [PDF 99-000-0030]. The latter observation is consistent with previous reports,[13,17] showing that cubic and hexagonal polymorphs may coexist in BSCF after annealing at 850 °C. Fig. 2 shows that the evolution of the cubic lattice parameter for the series BSCF-Z100·x is in accordance with Vegard's law up to the composition $x = 0.03$, which suggests that the solid solubility limit lies in the range 3–5 mol% of Zr. The latter is supported by combined TEM and EDX investigations conducted by Ravkina et al.[21] showing that Zr-rich phases crystallize at the grain boundaries of samples BSCF-Z100·x with $x \geq 0.05$.

Typical SEM micrographs of BSCF-Z100·x samples are given in Fig. 3, verifying that homogenous microstructures are obtained. From these micrographs porosities of less than 5% were extracted for all samples in the series. SEM and EDX analysis of the BSCF-Z10 specimen after thermal etching confirmed segregation of Zr-rich phases at the grain-boundaries. Table 1 lists grain sizes that were estimated from the SEM micrographs.

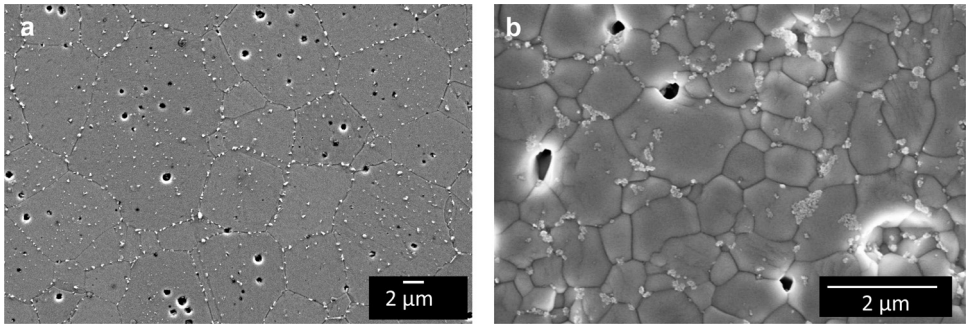

Fig. 3. Typical SEM micrographs of sintered BSCF-Z100·*x* ceramics: (a) BSCF-Z3 and (b) BSCF-Z10 (thermally etched at 950 °C for 20 min).

Table 2
Activation energy, Q (at 63 MPa), and average stress exponent, n, for creep of BSCF-Z100·*x*. Data were obtained from fitting experimental data (linear regression, Q and standard error) of the steady-state creep rate ($T \geq 850$ °C) to Eq. (2).

	n		Q [kJ/mol]	
	Heating	Cooling	Heating	Cooling
BSCF[a]	1.7 ± 0.2	–	530	340 ± 40
BSCF-Z1	2.0 ± 0.5	1.9 ± 0.1	570 ± 70	320
BSCF-Z3	1.5 ± 0.2	1.2 ± 0.2	730 ± 150	320 ± 10
BSCF-Z5	2.4 ± 0.6	–	660 ± 45	–
BSCF-Z10	4.0 ± 1.5	4.6 ± 0.5	845 ± 190	440 ± 25

[a] Data from Ref. 4.

From the results it is immediately apparent that substitution of (Co,Fe) by Zr severely suppresses grain growth. At similar sintering conditions (see experimental section), the grain size for BSCF-Z10 is less by a factor ~13 compared to that observed for pure BSCF. The observations are tentatively explained by a solute drag effect exerted by possible segregation of Zr to the grain boundaries (due to the charge and size mismatch with native (Co,Fe) ions in BSCF). At dopant concentrations in excess of the solid solubility limit, secondary phase pinning or dragging mechanism (Zener pinning) may contribute to the suppressed grain growth.

3.2. Creep measurements

Fig. 4 shows Arrhenius plots of the creep rates of compositions BSCF-Z3 and BSCF-Z10 upon heating and cooling. Similar results were obtained for other compositions in the BSCF-Z100·*x* series. For BSCF-Z3 a good agreement is noted with results obtained previously by Pećanac et al.[11] on sintered extruded tubes (porosity 6%, grain size 20 ± 8 µm) as illustrated in Fig. 4a, verifying an insignificant influence of the production route. A profound hysteresis in the creep rates was observed upon thermal cycling for all investigated compositions, which indicates that in the experimental range of dopant concentrations its origin is not influenced by the Zr dopant. As discussed above, the origin of the hysteresis in the creep rate for pure BSCF was explained previously by the material's phase instability below ~850 °C.[2,12] Activation energies, Q, and average stress exponents, n, obtained by fitting experimental data of the creep rate of compositions BSCF-Z100·*x*, at $T \geq 850$ °C, to Eq. (1) are listed in Table 2.

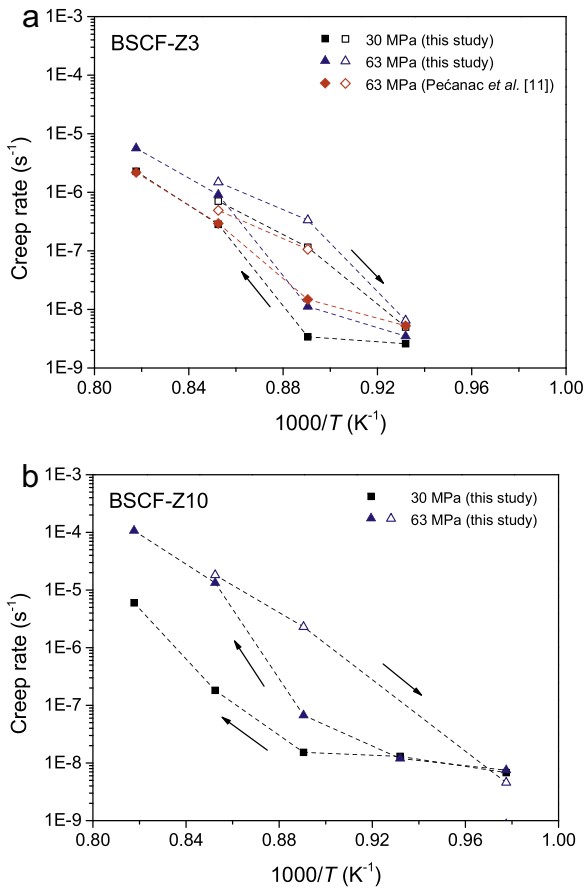

Fig. 4. Temperature dependence of the steady-state creep rate for (a) BSCF-Z3 and (b) BSCF-Z10 at nominal stresses of 30 and 63 MPa. The arrows indicate heating and cooling directions.

Due to the hysteresis in the creep rate the apparent activation energies Q for heating and cooling runs are found highly dissimilar. As hexagonal polymorphs are absent in pure BSCF when heated up to ~950 °C,[12] and polymorphism is induced only during long-term annealing below ~850 °C, the extracted values of Q from cooling curves are considered to reflect the activation energy of the creep rate of the cubic perovskite phase. Average values of Q extracted from data of cooling runs for pure BSCF,[4] BSCF-Z1 and BSCF-Z3 are in the range 320–340 kJ/mol. Good agreement is noted with the value of 350 kJ/mol extracted from

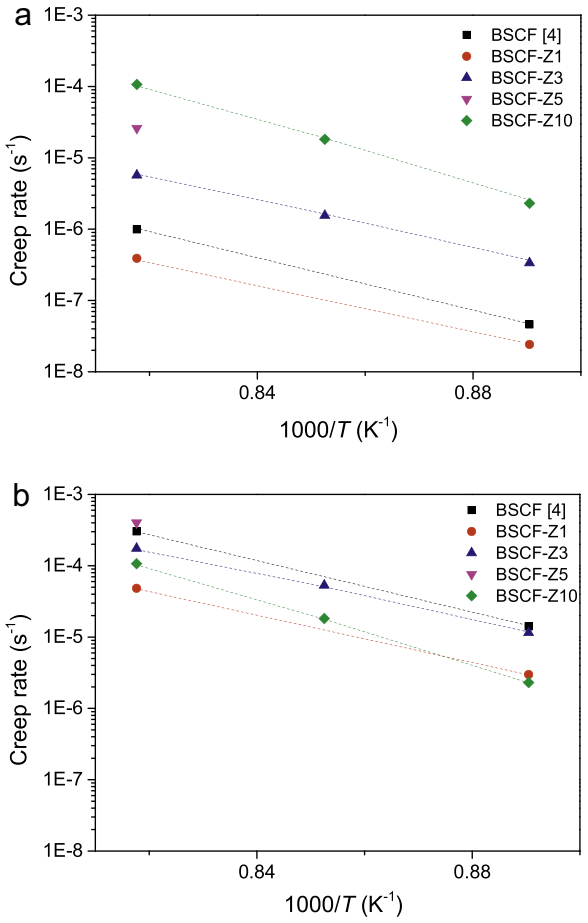

Fig. 5. Steady-state creep rate of BSCF-Z100·x, at $T \geq 850\,^{\circ}C$ (cooling runs), (a) before and (b) after normalization to grain size $d = 1\,\mu m$ (see main text).

data of sintered extruded tubes of BSCF-Z3 measured under similar conditions.[11] For BSCF-Z10 a slightly higher value of 440 kJ/mol is measured (see Table 2). The observed high activation energies resemble those measured for cation diffusion in perovskite oxides as determined from diffusion couple and isotope tracer experiments,[25–27] and exclude oxygen ions as the rate controlling species, noting that the activation energy for oxygen transport in BSCF ceramics has been reported to be below 50 kJ/mol.[2]

As can be seen from Table 2, the stress exponent n varies between 1.5 and 2, except for BSCF-Z10, suggesting a diffusion-aided creep mechanism for the compositions with lower Zr contents. Strictly speaking, the value of n is close to unity for diffusion creep, while for, e.g., dislocation creep, it is usually in the range of 3–8.[28–30] For pure BSCF (with grain size $29 \pm 11\,\mu m$) a value of $n = 1.7 \pm 0.5$ for $T > 800\,^{\circ}C$ was reported by Rutkowski et al.[4] Yi et al.[9] reported $n = 0.76 \pm 0.23$ for the lower stress regime 5–20 MPa. For BSCF-Z10, the stress exponent obtained in the current study takes a value of ~4, suggesting a change-over from diffusion to a dislocation creep mechanism at higher Zr contents. The grain size measured before and after test agreed within the limits of uncertainty ($1.0 \pm 0.3\,\mu m$ and $1.5 \pm 0.5\,\mu m$, respectively), and no specific grain orientation could be verified by electron backscatter diffraction (EBSD). An alternative explanation would be that grain boundary pinning by secondary (Ba,Sr)ZrO_3 phases contributes to diffusional creep in BSCF-Z10. As for a diffusion creep mechanism the creep rate depends on grain size, the measured creep rates were normalized to a grain diameter of 1 μm. A value $p = 1.7$ was used for the inverse grain size exponent in the calculations, which value was taken from our previous study on the grain size-dependence of the creep rate of pure BSCF.[4] Fig. 5a and b show the creep rates (cooling curves), at $T \geq 850\,^{\circ}C$, of compositions BSCF-Z100·x before and after normalization, respectively. Figure 5b reveals that the normalized creep rates varies little for the different compositions, which finding supports the conclusion that under this conditions of stress and temperature diffusional creep is the predominant mechanism for creep in these materials. Only through its suppression of the grain growth, Zr substitution of (Co,Fe) in BSCF leads to an enhancement of the creep rate relative to that observed for the pure material.

4. Conclusions

Zr substitution of (Co,Fe) in BSCF is found to suppress grain growth significantly. X-ray diffraction and microstructural observations further support a solid solubility limit of ZrO_2 in BSCF-Z100·x between $0.03 < x < 0.05$. Evidence is found for segregation of (Ba,Sr)ZrO_3 at the grain boundaries for compositions $x \geq 0.05$. The suppressed grain growth in compositions BSCF-Z100·x relative to that of parent BSCF is attributed to a solute and/or particle drag (Zener pinning) mechanism.

The substitution of Zr is not found to have any significant effect on the thermal hysteresis of the creep behavior as observed for pure BSCF. Diffusional creep is confirmed as the predominant mechanism for the creep, at $T \geq 850\,^{\circ}C$, in BSCF-Z100·x. This is supported by the high activation energies and low stress exponents observed for the steady-state creep rate, and by the fact that the grain-size-normalized creep rates of the different compositions BSCF-Z100·x ($x = 0$, 0.01, 0.03, 0.05 and 0.1) coincide within experimental error.

Acknowledgements

Financial support from the Helmholtz Association of German Research Centers (Initiative and Networking Fund) through the Portfolio-topic MEM-BRAIN is gratefully acknowledged. The authors express their gratitude to Ms. T. Osipova, Mr. R. Küppers and Mr. J. Mönch for technical assistance, to Dr. E. Wessel and Dr. D. Grüner for SEM analysis, and to Mr. M. Ziegner for XRD analysis. Finally, Dr. G. Pećanac is gratefully acknowledged for fruitful discussions.

References

1. Baumann S, Serra JM, Lobera MP, Escolastico S, Schulze-Küppers F, Meulenberg WA. Ultrahigh oxygen permeation flux through supported $Ba_{0.5}Sr_{0.5}Co_{0.8}Fe_{0.2}O_{3-\delta}$ membranes. *J Membr Sci* 2011;**377**:198–205.
2. Shao Z, Yang W, Cong Y, Dong H, Tong J, Xiong G. Investigation of the permeation behavior and stability of a $Ba_{0.5}Sr_{0.5}Co_{0.8}Fe_{0.2}O_{3-\delta}$ oxygen membrane. *J Membr Sci* 2000;**172**:177–88.

3. Niedrig C, Taufall S, Burriel M, Menesklou W, Wagner S, Baumann S, et al. Thermal stability of the cubic phase in $Ba_{0.5}Sr_{0.5}Co_{0.8}Fe_{0.2}O_{3-\delta}$ (BSCF). *Solid State Ion* 2011;**197**:25–31.
4. Rutkowski B, Malzbender J, Beck T, Steinbrech RW, Singheiser L. Creep behaviour of tubular $Ba_{0.5}Sr_{0.5}Co_{0.8}Fe_{0.2}O_{3-\delta}$ gas separation membranes. *J Eur Ceram Soc* 2011;**31**:493–9.
5. Dyer P, Richards R, Russek SL, Taylor D. Ion transport membrane technology for oxygen separation and syngas production. *Solid State Ion* 2000;**34**:21–33.
6. Czyperek M, Zapp P, Bouwmeester HJM, Modigell M, Ebert K, Voigt I, et al. Gas separation membranes for zero-emission fossil power plants: MEM-BRAIN. *J Membr Sci* 2010;**359**:149–59.
7. Pećanac G, Baumann S, Malzbender J. Mechanical properties and lifetime predictions for $Ba_{0.5}Sr_{0.5}Co_{0.8}Fe_{0.2}O_{3-\delta}$ membrane material. *J Membr Sci* 2011;**385–386**:263–8.
8. Lipińska-Chwałek M, Pećanac G, Malzbender J. Creep behaviour of membrane and substrate materials for oxygen separation units. *J Eur Ceram Soc* 2013;**33**:1841–8.
9. Yi JX, Lein HL, Grande T, Yakovlev S, Bouwmeester HJM. High-temperature compressive creep behaviour of the perovskite-type oxide $Ba_{0.5}Sr_{0.5}Co_{0.8}Fe_{0.2}O_{3-\delta}$. *Solid State Ion* 2009;**180**:1564–8.
10. Rutkowski B, Malzbender J, Steinbrech RW, Beck T, Bouwmeester HJM. Influence of thermal history on the cubic-to-hexagonal phase transformation and creep behaviour of $Ba_{0.5}Sr_{0.5}Co_{0.8}Fe_{0.2}O_{3-\delta}$. *J Membr Sci* 2011;**381**:221–5.
11. Pećanac G, Kiesel L, Malzbender J. Steady-state creep of porous and an extended analysis on the creep of dense BSCFZ perovskite. *J Membr Sci* 2014;**456**:134–8.
12. Liang F, Jiang H, Luo H, Caro J, Feldhoff A. Phase stability and permeation behavior of a dead-end $Ba_{0.5}Sr_{0.5}Co_{0.8}Fe_{0.2}O_{3-\delta}$ tube membrane in high-purity oxygen production. *Chem Mater* 2011;**23**:4765–72.
13. Švarcová S, Wiik K, Tolchard J, Bouwmeester HJM, Grande T. Structural instability of cubic perovskite $Ba_xSr_{1-x}Co_{1-y}Fe_yO_{3-\delta}$. *Solid State Ion* 2008;**178**:1787–91.
14. Müller DN, De Souza RA, Weirich TE, Röhrens D, Mayer J, Martin M. A kinetic study of the decomposition of the cubic perovskite-type oxide $Ba_xSr_{1-x}Co_{0.8}Fe_{0.2}O_{3-\delta}$ (BSCF) ($x = 0.1$ and 0.5). *Phys Chem Chem Phys* 2010;**12**:10320–8.
15. Efimov K, Xu Q, Feldhoff A. Transmission electron microscopy study of $Ba_{0.5}Sr_{0.5}Co_{0.8}Fe_{0.2}O_{3-\delta}$ perovskite decomposition at intermediate temperatures. *Chem Mater* 2010;**22**:5866–75.
16. Müller P, Störmer H, Meffert M, Dieterle L, Niedrig C, Wagner SF, et al. Secondary phase formation in $Ba_{0.5}Sr_{0.5}Co_{0.8}Fe_{0.2}O_{3-\delta}$ studied by electron microscopy. *Chem Mater* 2013;**25**:564–73.
17. Haworth P, Smart S, Glasscock J, Diniz da Costa JC. Yttrium doped BSCF membranes for oxygen separation. *Sep Purif Technol* 2011;**81**:88–93.
18. Fang SM, Yoo CY, Bouwmeester HJM. Performance and stability of niobium-substituted $Ba_{0.5}Sr_{0.5}Co_{0.8}Fe_{0.2}O_{3-\delta}$ membranes. *Solid State Ion* 2011;**195**:1–6.
19. Meng X, Yang N, Meng B, Tan X, Ma Z, Liu S. Zirconium stabilized $Ba_{0.5}Sr_{0.5}(Co_{0.8-x}Zr_x)Fe_{0.2}O_{3-\alpha}$ perovskite hollow fibre membranes for oxygen separation. *Ceram Int* 2011;**37**:2701–9.
20. Yakovlev S, Yoo CY, Fang S, Bouwmeester HJM. Phase transformation and oxygen equilibration kinetics of pure and Zr-doped $Ba_{0.5}Sr_{0.5}Co_{0.8}Fe_{0.2}O_{3-\delta}$ perovskite oxide probed by electrical conductivity relaxation. *Appl Phys Lett* 2010;**96**:254101–3.
21. Ravkina O, Klande T, Feldhoff A. Investigation of Zr-doped BSCF perovskite membrane for oxygen separation in the intermediate temperature range. *J Solid State Chem* 2013;**201**:101–6.
22. Pećanac G, Kiesel L, Kriegel R, Malzbender J. Comparison of thermo-mechanical characteristics of non-doped and 3 mol% B-site Zr-doped $Ba_{0.5}Sr_{0.5}Co_{0.8}Fe_{0.2}O_{3-\delta}$. *Ceram Int* 2014;**40**:1843–50.
23. Pfaff EM, Kaletsch A, Broeckmann C. Design of a mixed ionic/electronic conducting oxygen transport membrane pilot module. *Chem Eng Technol* 2012;**35**:455–63.
24. Bretheau T, Castaing J, Rabier J, Veyssiere P. Dislocation motion and high temperature plasticity of binary and ternary oxides. *Adv Phys* 1979;**28**:835–1014.
25. Palcut M, Wiik K, Grande T. Cation self-diffusion and nonstoichiometry of lanthanum manganite studied by diffusion couple measurements. *J Phys Chem B* 2007;**111**:813–22.
26. Palcut M, Wiik K, Grande T. Cation self-diffusion in $LaCoO_3$ and La_2CoO_4 studied by diffusion couple experiments. *J Phys Chem B* 2007;**111**:2299–308.
27. Smith JB, Norby T. On the steady-state oxygen permeation through $La_2NiO_{4+\delta}$ membranes. *J Electrochem Soc* 2006;**153**:A233–8.
28. Nabarro FRN. *Report of a conference on strength of solids*. London: Physical Society; 1948. p. 75.
29. Herring C. Diffusional viscosity of a polycrystalline solid. *J Appl Phys* 1950;**2**:437–45.
30. Coble RL. A model for boundary diffusion controlled creep in polycrystalline materials. *J Appl Phys* 1963;**34**:1679–83.